JACS
JOURNAL OF THE AMERICAN CHEMICAL SOCIETY

Article

pubs.acs.org/JACS

Modular Riboswitch Toolsets for Synthetic Genetic Control in Diverse Bacterial Species

Christopher J. Robinson,[†,‡] Helen A. Vincent,[†,‡,∥] Ming-Cheng Wu,[†,‡,∥] Phillip T. Lowe,[†,‡] Mark S. Dunstan,[‡,§] David Leys,[‡,§] and Jason Micklefield*[,†,‡]

[†]School of Chemistry, [‡]Manchester Institute of Biotechnology and [§]Faculty of Life Sciences, The University of Manchester, 131 Princess Street, Manchester M1 7DN, United Kingdom

Supporting Information

ABSTRACT: Ligand-dependent control of gene expression is essential for gene functional analysis, target validation, protein production, and metabolic engineering. However, the expression tools currently available are difficult to transfer between species and exhibit limited mechanistic diversity. Here we demonstrate how the modular architecture of purine riboswitches can be exploited to develop orthogonal and chimeric switches that are transferable across diverse bacterial species, modulating either transcription or translation, to provide tunable activation or repression of target gene expression, in response to synthetic non-natural effector molecules. Our novel riboswitch−ligand pairings are shown to regulate physiologically important genes required for bacterial motility in *Escherichia coli* and cell morphology in *Bacillus subtilis*. These findings are relevant for future gene function studies and antimicrobial target validation, while providing new modular and orthogonal regulatory components for deployment in synthetic biology regimes.

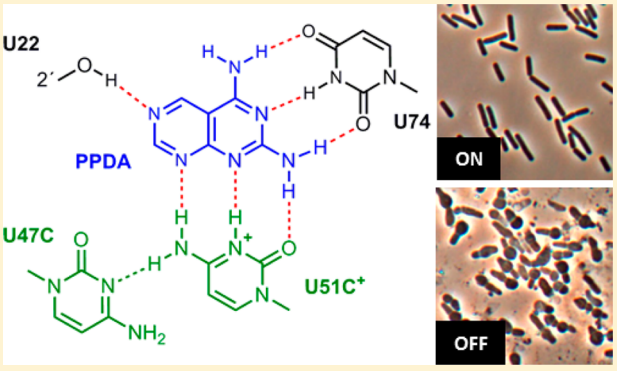

INTRODUCTION

Riboswitches are small structured mRNA elements, present across all domains of life, which regulate gene expression in response to specific small-molecule ligands.[1,2] Riboswitches are found with the highest frequency in the 5′-UTR of bacterial mRNAs, and possess a modular architecture comprised of two distinct, but overlapping, domains. The aptamer domain selectively binds a target metabolite, resulting in a conformational change which is communicated to an adjacent expression platform that determines the gene expression outcome.[3]

Riboswitches are attractive targets in the development of small-molecule responsive gene-expression systems for gene functional studies, synthetic biology and biotechnological applications. RNA-based gene regulatory control would be complementary to, and could offer advantages over, conventional protein-based strategies. Riboswitches function through protein-independent mechanisms, and therefore should possess greater transferability between species, compared with protein-based expression systems. Also, riboswitches have been shown to control transcription, translation, mRNA self-cleavage or pre-mRNA splicing, with both inducible (ON) and repressible (OFF) variants identified, maximizing the potential for downstream applications. Most protein-based expression systems are induced by specific effector molecules, while fewer systems are available that can conditionally repress gene expression. The inherent modularity of riboswitches allows for the exchange of aptamer domains and expression platforms between different riboswitches,[4,5] to provide chimeric switches that can deliver a diverse range of expression outputs in response to different ligands. Riboswitches can also be deployed in serial arrangements, to afford more digital control over gene expression, and to create regulatory elements which act as Boolean logic gates.[1,6] Finally, while many established protein-based expression systems exhibit *all-or-none* expression profiles,[7,8] riboswitches typically exhibit precise dose-dependent control over gene expression.[9]

The potential of RNA aptamers as gene regulatory tools was recognized before the discovery of natural riboswitches. Synthetic aptamers, which can be selected from randomized RNA libraries to bind any small molecule of interest, have been used to control gene expression through a wide-variety of mechanisms in both bacterial and eukaryotic hosts.[10,11] Further advances in the development of high-throughput genetic screens and selection strategies have been used for the *de novo* creation of riboswitches with desirable gene regulatory functions.[12−16] Despite these successes, only a very limited range of *in vitro*-selected aptamers have been successfully exploited in artificial riboswitch applications.[11] There is therefore a pressing need to increase the diversity of RNA aptamers which can be used for *in vivo* regulatory purposes. Natural riboswitch aptamers are ideally suited to this function

Received: March 21, 2014
Published: June 27, 2014

dx.doi.org/10.1021/ja502873j | J. Am. Chem. Soc. 2014, 136, 10615−10624

as they have evolved to interface with a wide-range of structurally diverse expression platforms; and several applications utilizing natural aptamers have been reported.[4,5,17,18] However, these aptamers bind cellular metabolites, and therefore their use as generic control elements can be compromised by fluctuations in intracellular metabolite concentrations, and the exogenous addition of these compounds could negatively impact normal cellular function. Recently, we provided a potential solution to this problem by re-engineering the adenine responsive *add* A-riboswitch (Figure 1A).[19] Ligand binding to the aptamer domain of this riboswitch releases the ribosome-binding site and start codon from an adjacent repressor stem, thereby allowing for translation of the associated mRNA.[20,21] The re-engineered riboswitches no longer responded to adenine (**1**), but instead could be regulated by the synthetic non-natural ligands, ammeline (**2**, Amm) and 5-azacytosine (**3**, AzC).[19] However, the orthogonal riboswitch-ligand pairings that we developed, M6″−Amm and M6C″−AzC, were notably weaker at inducing reporter gene expression and exhibited greatly reduced affinities when compared with the parental *add* A-riboswitch. Furthermore, the ligands Amm and AzC have poor aqueous solubility, limiting the scope for subsequent *in vivo* applications. Here we describe the discovery of new riboswitch−synthetic ligand pairings which are used to create synthetic regulatory components that are orthogonal, modular, and transferable, enabling functional control of physiologically important genes in both Gram-negative and Gram-positive bacteria.

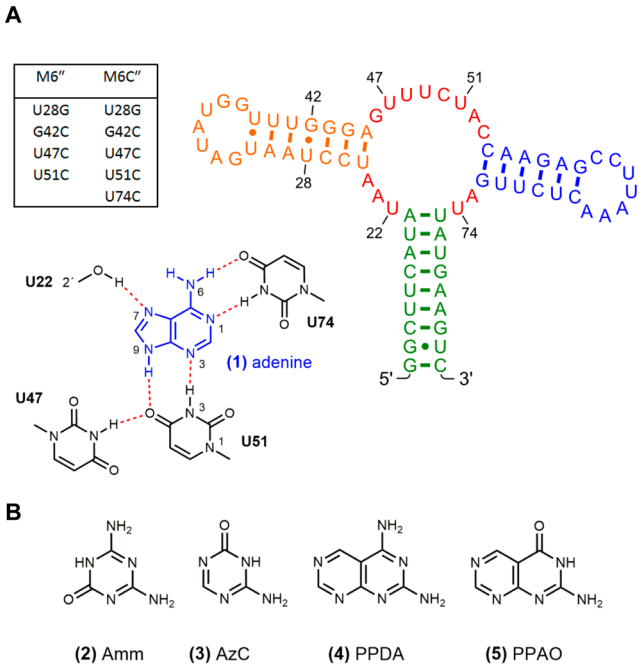

Figure 1. Riboswitches and ligands used in this study. (A) Secondary structure of the *add* A-riboswitch aptamer domain, with the P1 stem (green), P2-L1 stem-loop (orange), P3-L2 stem-loop (blue), and three-way junction (red). Key residues are labeled, with mutations tabulated and hydrogen bond interactions of adenine (blue) with the *add* A-aptamer shown below. (B) Chemical structures of several key compounds are also shown.

RESULTS AND DISCUSSION

Orthogonal Riboswitch Ligands with Superior *in vivo* Gene Induction Properties. Our previous crystal structure of the orthogonal riboswitch M6C″ in complex with AzC[19] revealed key structural differences within the ligand-binding pocket when compared with the parental *add* A-riboswitch structure (Figure 1A and Figure S1). In particular, there was a 1.8 Å lateral movement of C51, relative to U51 in the parental structure, to allow for productive H-bonding with the AzC ligand. This structure suggests that "adaptive ligand binding"[22] mediated by local flexibility in the ligand-binding pocket may facilitate the binding of more structurally diverse ligands than first anticipated. With this in mind, a wider-range of heterocyclic compounds were screened as potential M6″ or M6C″ ligands.[19]

The fluorescence of *Escherichia coli* cells, in which eGFP was placed under the translational control of the M6″, M6C″ or parental *add* A-riboswitch (Figure 2A), was measured in the presence of potential ligands from a library of heterocyclic compounds. From this assay two promising riboswitch inducer compounds emerged, pyrimido[4,5-*d*]pyrimidine-2,4-diamine

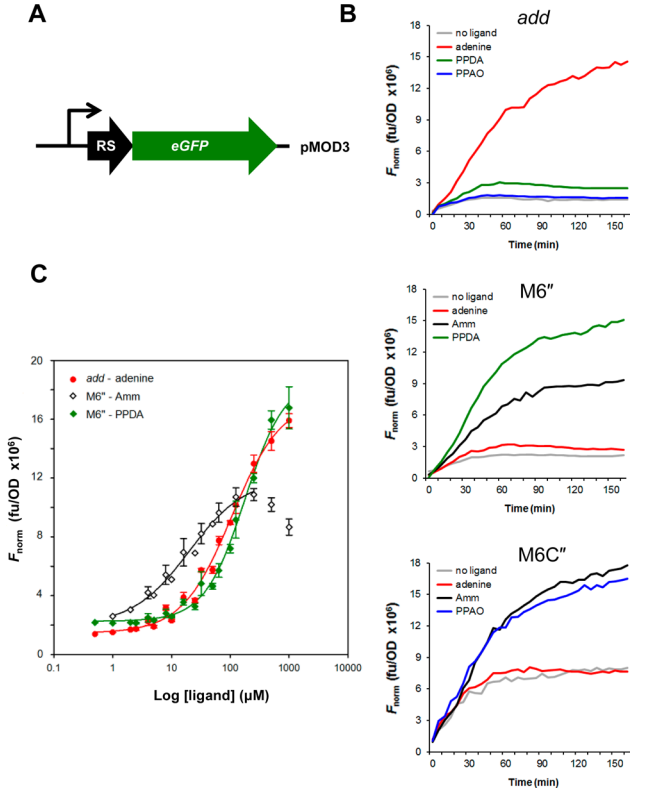

Figure 2. Ligand-dependent eGFP expression in *E. coli*. (A) The expression construct, composed of the *lac* promoter (black line arrow) upstream of an inducible riboswitch (RS; black block arrow), controlling expression of the eGFP gene (green block arrow). (B) Induction of eGFP expression controlled by the *add*, M6″ and M6C″ riboswitches after treatment with 500 μM of the indicated ligands. Fluorescence measurements were normalized for cell density (F_{norm}), and represent the mean of four repeat experiments. (C) Dose-dependent eGFP expression for the riboswitch−ligand pairs indicated. Normalized fluorescence is shown 160 min after ligand addition, as the mean of at least three repeat experiments, with error bars indicating standard error. Curves were fitted using a four-parameter logistic function.

dx.doi.org/10.1021/ja502873j | J. Am. Chem. Soc. 2014, 136, 10615−10624

(**4**, PPDA) and 2-aminopyrimido[4,5-*d*]pyrimidin-4(3*H*)-one (**5**, PPAO) (Figure 1B and Figure S2). PPDA induced the M6″ riboswitch, yielding an eGFP fluorescence response of 15.1 × 10^6 fu/OD (normalized fluorescence units, Figure 2B). This was a marked improvement on Amm induction of M6″ (9.4 × 10^6 fu/OD), and was equivalent to the fluorescence level observed for adenine induction of the parental *add* A-riboswitch (14.5 × 10^6 fu/OD). The compound PPAO induced the M6C″ riboswitch, yielding similar levels of eGFP expression as were observed for Amm induction of M6C″ (16.5 × 10^6 and 17.8 × 10^6 fu/OD respectively, Figure 2B). Induction factors were calculated by dividing the fluorescence levels observed in the presence of ligand, by the basal levels observed in the absence of ligand. Adenine induced a 10.3-fold increase in eGFP expression (at 500 μM ligand concentration) from the *add* A-riboswitch. In the same assay, M6″−PPDA induced a 7.0-fold increase in eGFP levels (at 500 μM ligand concentration), a clear improvement on the 4.3-fold induction observed for M6″−Amm. The difference in induction factors observed between M6″−PPDA and parental riboswitch−ligand pairing was due to the basal expression being slightly higher for the M6″-eGFP construct (2.2 × 10^6 and 1.4 × 10^6 fu/OD respectively), as the absolute fluorescence levels in the presence of ligand were almost identical. Basal expression was particularly high for the M6C″-eGFP construct, which we speculate is a consequence of induction by endogenous guanosine and 2′-deoxyguanosine, as noted previously.[19] Importantly, neither PPDA nor PPAO induced eGFP expression from the parental *add* A-riboswitch, and likewise adenine did not induce either the M6″ or M6C″ riboswitches (Figure 2B), confirming the *in vivo* orthogonality of these three riboswitch−ligand pairings.

A further notable property of M6″−PPDA was that the initial rate of eGFP expression was greater from this pairing than from either M6″−Amm or the parental pairing, reaching saturation at around 17 × 10^6 fu/OD after just 90 min with 1 mM ligand (Figure S3). It is unclear whether this enhanced initial rate of induction is a result of greater uptake or bioavailability of the PPDA ligand, or whether it is due to the kinetics of riboswitch−ligand interactions. Nevertheless, an enhanced rate of ligand induction is a desirable property for synthetic gene expression tools, reducing batch times and potentially improving yields by minimizing the exposure time of gene products to degradatory pathways. M6″−PPDA was also found to display excellent dose-dependent control over eGFP expression (Figure 2C), almost identical to that observed for adenine induction of the parental *add* A-riboswitch, with EC_{50} values of 177 and 107 μM respectively. Notably, eGFP expression levels induced by Amm reached a maximum at 250 μM ligand concentration, most likely due to negative effects observed on cell growth at higher concentrations (Figure 2C). In contrast, eGFP expression from the same M6″ construct remained dose-dependent up to 1 mM concentration of PPDA with no negative effects on cell growth, and a maximum induction factor of 8.3 calculated from the fitted data. Although this induction factor appears modest when compared with the best-performing artificial riboswitches,[13] it should be noted that the expression platform for this riboswitch evolved specifically to control adenine deaminase expression levels in *Vibrio vulnificus*, and no attempt was made here to optimize the dynamic range of expression. The M6″ aptamer should equally be amenable to FACS-based screening processes to identify new expression platforms with optimized ribosome-binding sites. However, for many applications, including gene functional analysis, large induction factors are not necessarily ideal; it is far more desirable to be able to tune the levels of gene expression in a dose-dependent manner over an accessible range of inducer concentrations.

Enhanced Affinity and Novel Interactions of Orthogonal Riboswitch−Ligand Pairings. The interactions of PPDA, PPAO and adenine with *in vitro* transcribed riboswitch aptamer domains were explored using isothermal titration calorimetry (ITC). Adenine bound to the parental *add* A-aptamer with an apparent equilibrium dissociation constant (K_D) of 43 nM (Figure 3A). The synthetic ligand PPAO bound

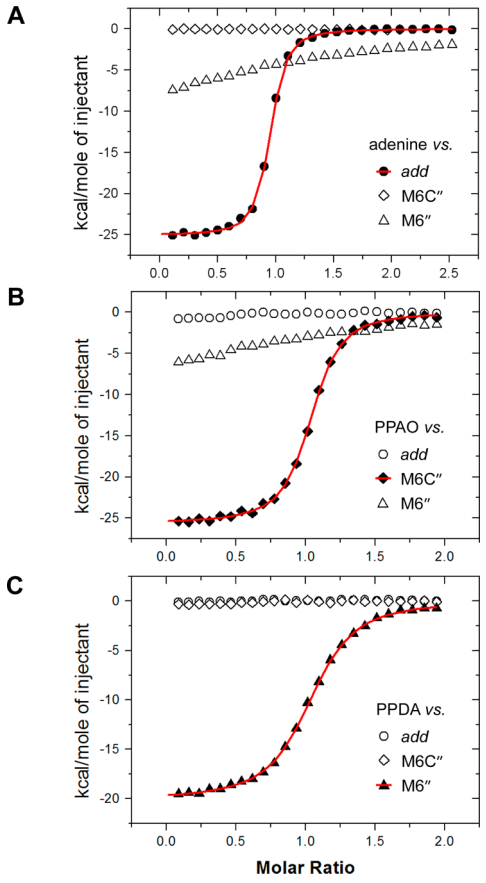

Figure 3. ITC analysis of aptamer−ligand interactions. Titration of adenine (A), PPAO (B), or PPDA (C) into *add* (circles), M6C″ (diamonds), or M6″ (triangles) riboswitch aptamer solutions. Experiments were conducted at 25 °C in HEPES buffer. Curves were fitted in Origin, using the supplied software (MicroCal). For thermodynamic parameters see Table S1.

to the mutant M6C″ aptamer with an apparent K_D of just 95 nM (Figure 3B), almost as strong an interaction as the parental pairing, and notably stronger than the 1 μM K_D values previously determined for Amm and AzC binding to M6C″.[19] Similarly, the M6″ aptamer bound PPDA with an apparent K_D of 213 nM (Figure 3C), a much stronger interaction than that characterized previously for M6″−Amm (1.2 μM apparent K_D).[19] Importantly, PPDA does not bind to M6C″ or *add* A-aptamers, PPAO shows no discernible affinity for either M6″ or *add* A-aptamers, while adenine exhibits no appreciable affinity for either M6″ or M6C″. This excellent *in vitro* binding orthogonality is consistent with the *in vivo* expression data (Figure 2B). Both PPDA binding to the M6″ aptamer, and PPAO binding to the M6C″ aptamer, were driven entirely by

dx.doi.org/10.1021/ja502873j | J. Am. Chem. Soc. 2014, 136, 10615−10624

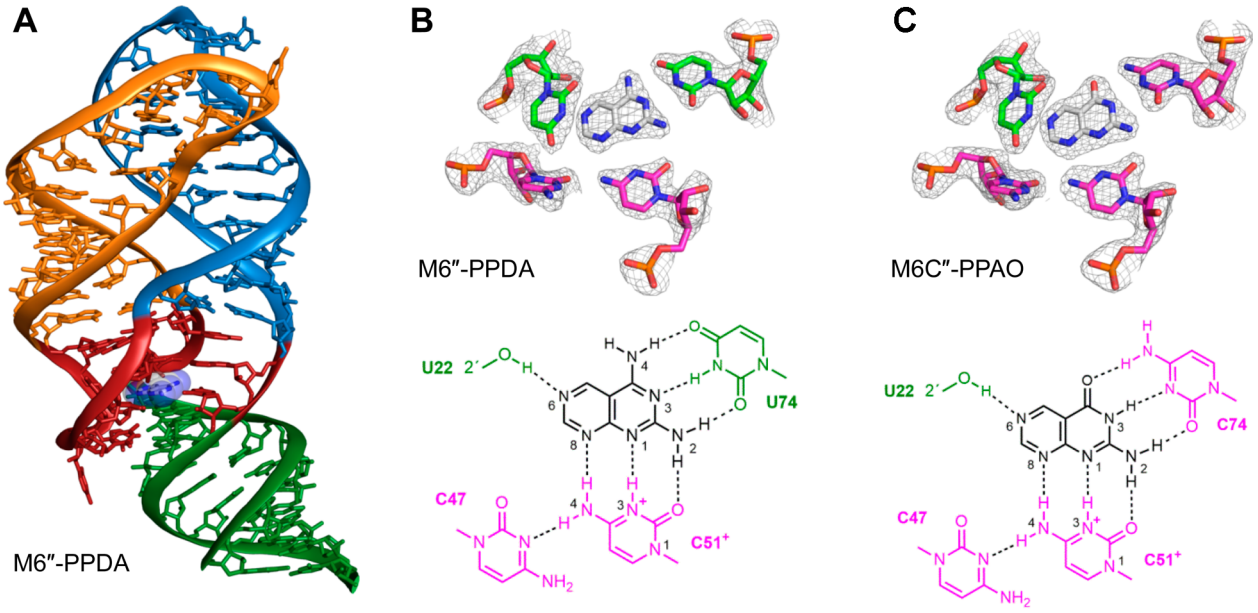

Figure 4. Structures of aptamer–ligand complexes. (A) Model of the M6″–PPDA complex solved by X-ray crystallography. PPDA is shown in stick representation within transparent spheres. M6″ aptamer is shown in stick representation, with the phosphodiester backbone highlighted as a ribbon. Secondary structure elements are colored as in Figure 1. (B) Top: Detail of the ligand-binding pocket of M6″–PPDA. Ligand and aptamer residues are depicted as sticks within a $2mF_0$-DF_c sigma-A weighted map, contoured at 1 σ. Carbon atoms in the ligand are highlighted in white, while those of the aptamer are shown in pink (mutated from wild-type) or green (nonmutated residues). Bottom: H-bonding model of PPDA binding to M6″, based on the crystal structure. Proposed H-bonds are shown as black dashed lines. (C) Detail of the ligand-binding pocket of M6C″–PPAO, and H-bonding model of PPAO binding to M6C″.

strong enthalpic contributions, with similar thermodynamic parameters to those observed for adenine binding to the parental *add* A-aptamer (Table S1).

On the basis of the previous structure of the M6C″–AzC complex,[19] it was anticipated that a lateral movement of C51 away from C47 would be required for the M6″ and M6C″ aptamers to bind PPDA and PPAO, respectively (Figure S1). To investigate the modes of binding, the M6″–PPDA and M6C″–PPAO complexes where crystallized under conditions described previously,[19,21] and structures were solved to 2.2 Å using the molecular replacement method (Figure 4A, Figure S4 and Table S2A). It is clear from structural alignment (Figure S4 and Table S2B) that both M6″–PPDA and M6C″–PPAO share a greater similarity with the parental *add* A-aptamer complex[21] (RMSD 0.65 and 0.47 Å, respectively) than with the M6C″–AzC complex[19] (RMSD 1.8 and 1.7 Å, respectively), indicating that these pyrimido[4,5-*d*]pyrimidine (PP) ligands induce less structural perturbation of the RNA aptamers. The increased π-surface area of the bicyclic PP ligands, compared with monocyclic AzC, also affords more extensive π-stacking interactions with the U22–A52 and A21–U75 base pairs above and below the ligands. As expected, U74 of M6″ and C74 of M6C″ determine specificity, engaging in three H-bonds with the "diamino-face" of PPDA and the "guanine-face" of PPAO, respectively (Figure 4B,C). A further H-bond is evident between the 2′-OH of U22 and N6 in the PP ligands, analogous to the H-bond observed between U22 and N7 of adenine in the parental structure (Figure 1). The electron density clearly positions C51 adjacent to C47 in both the M6″–PPDA and M6C″–PPAO structures, such that the N4 exocyclic amine group of C51 can H-bond with N3 of C47 (Figures 4B,C). However, since there is no lateral movement of C51 relative to C47, this places N3 of C51 within 2.9 Å of N1 in the PP ligand in both structures, leading to adverse lone-pair clashes, which we rationalize would necessitate protonation at this position.

To determine whether binding of the PP ligands to their respective aptamer domains was dependent upon protonation (proton-linkage), ITC was used to measure changes in the observed enthalpy of ligand binding (ΔH_{obs}) in buffer systems with different enthalpies of ionization (ΔH_{ion}).[23,24] If a ligand binding event is associated with the uptake of protons from the buffer, then there will be a linear relationship between ΔH_{obs} and ΔH_{ion} (Figure 5, eq 1), with the gradient of the line being equivalent to N_{H+}, the number of protons taken up by the complex.[25−27] For the interaction of adenine with the parental *add* A-aptamer, ΔH_{obs} was independent of ΔH_{ion}, which indicates that adenine binding was not associated with proton uptake (Figure 5, Figure S5 and Table S3). In contrast, for the M6″–PPDA and M6C″–PPAO interactions there was a clear influence of the buffer systems used on ΔH_{obs}; the plots of ΔH_{obs} vs ΔH_{ion} were linear (Figure 5), with positive gradients (N_{H+}) of 0.81 and 0.85, respectively, consistent with the net uptake of approximately one proton for each aptamer–ligand complex formed. These data support our proposed binding-site models, whereby a proton sits between N3 of the C51 residue and N1 of the PP ligands (Figures 4B,C); proton-linkage represents a novel mechanism of riboswitch ligand recognition, which has not been observed among the natural riboswitch–ligand interactions studied to date.

Controlling *E. coli* Cell Motility. To demonstrate the potential advantages of titratable orthogonal riboswitches for gene function studies, we sought to control expression of the native *E. coli* gene *cheZ* using the optimal M6″–PPDA pairing. CheZ is a phosphatase which is essential for regulating *E. coli* cell motility[28] (see Figure S6), and has been exploited previously as a selectable marker to identify synthetic riboswitches that function with artificially selected ap-

dx.doi.org/10.1021/ja502873j | J. Am. Chem. Soc. 2014, 136, 10615−10624

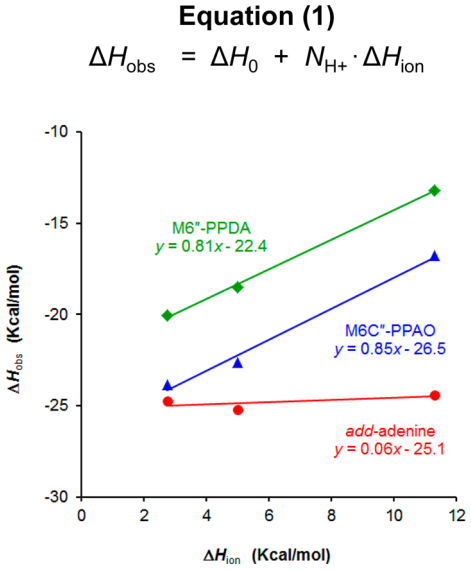

Figure 5. Investigation of proton-linkage to riboswitch ligand binding by ITC. Experiments were performed at 25 °C in PIPES (ΔH_{ion} = 2.74), HEPES (ΔH_{ion} = 5.01), or TRIS (ΔH_{ion} = 11.3) buffer. ITC binding curves and thermodynamic parameters are presented in Figure S5 and Table S3.

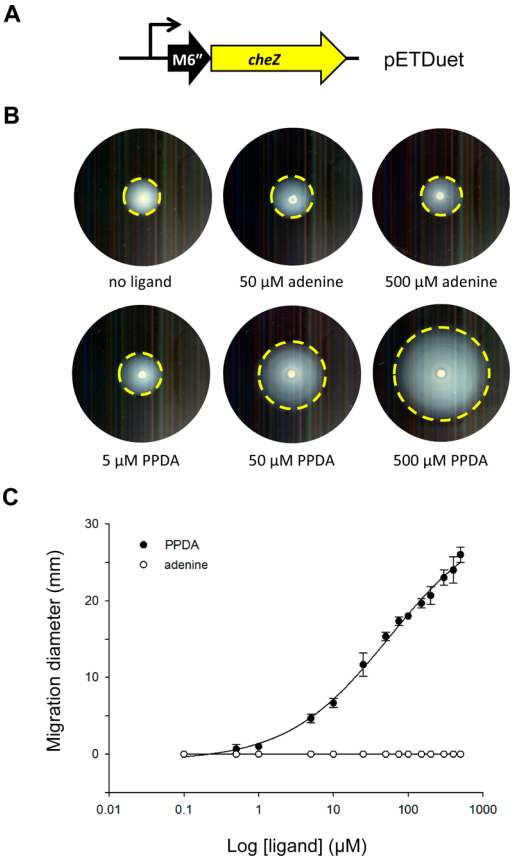

Figure 6. Dose-dependent regulation of *cheZ* expression controls *E. coli* motility. (A) The *cheZ* expression construct, comprised of the *lac* promoter (black line arrow) upstream of the inducible M6″ riboswitch (black block arrow), controlling expression of the *cheZ* gene (yellow block arrow). (B) Agar motility plates for a Δ*cheZ* strain of *E. coli* carrying the *cheZ* expression construct. Ligand concentrations are indicated. Yellow-dashed circles indicate the visual range of cell migration after 24 h at 25 °C. (C) Cell migration was measured for motility plates covering a range of adenine (open circles) or PPDA (filled circles) concentrations (see Figure S7). Data represent the mean of three repeat experiments, with error bars indicating standard deviation. Curves were fitted using a four-parameter logistic function.

tamers.[16,29] Therefore, we chose to clone the *cheZ* gene from *E. coli*, downstream of the M6″ riboswitch, in the medium copy number plasmid pETDuet-1 (Figure 6A). This construct was used to transform a *cheZ* deletion strain of *E. coli*, and the resulting cells were assayed for motility on semisolid media plates containing ligand. A clear response of the transformed cells to PPDA was observed, with a migration diameter of 26 mm for cells on plates containing 500 μM PPDA (Figure 6B). Notably, these cells exhibit dose-dependent cell migration in response to PPDA (Figure S7), with a sigmoidal trend over the range of concentrations tested (0.1 μM to 500 μM, Figure 6C). PPDA controls CheZ expression levels, and therefore the extent to which motility is promoted over the time-course of the experiments. In contrast, no migration of these cells was observed in response to adenine over the same concentration range, clearly demonstrating the *in vivo* orthogonality of the M6″ riboswitch. Re-engineered riboswitches which provide dose-dependent control of bacterial motility, such as those described in this study, could prove to be valuable tools for research in fields where bacterial motility is of central importance.

Orthogonal "Transcriptional OFF" Riboswitches. To demonstrate the transferability of re-engineered riboswitch tools between bacterial species, we sought to exploit the inherent modular architecture of riboswitches[4,5,17,18] to create new orthogonal switches that function in diverse bacterial species, and which provide alternative genetic outputs. Our strategy involved fusing the aptamer domain of M6″ to the expression platform of the *xpt* G-riboswitch from *Bacillus subtilis*.[30,31] It was envisaged that this would effectively transform the PPDA-sensing "translational ON" switch, derived from a Gram-negative bacterium, into a "transcriptional OFF" switch which would function in Gram-positive bacteria. The P1-stem of the *xpt* G-riboswitch includes five nucleotides (the switching sequence) which form part of the expression platform in the ON-state when ligand is absent (Figure S8), but which are not involved in ligand recognition. Utilizing this natural boundary, we generated constructs in which the β-galactosidase gene (*lacZ*) was placed under the transcriptional control of either the natural *xpt* G-riboswitch (*xpt*/*xpt*), a chimeric riboswitch composed of the *add* A-aptamer domain and the *xpt* G-riboswitch expression platform (*add*/*xpt*), or a chimeric riboswitch composed of the M6″-aptamer domain and the *xpt* G-riboswitch expression platform (M6″/*xpt*) (Figure 7A). These constructs were integrated into the *B. subtilis* chromosome at the *amyE* locus to create three different reporter strains. As expected, *lacZ* expression was repressed in a dose-dependent manner in the *xpt*/*xpt* strain upon the addition of guanine with an EC_{50} of 28 ± 2 μM (Figure 7B), while no repression was observed when adenine or PPDA was added. For the chimeric riboswitches, *lacZ* expression was repressed upon addition of the respective cognate ligands, with EC_{50} values of 120 ± 10 μM adenine for *add*/*xpt* and ca. 500 μM PPDA for M6″/*xpt* (Figure 7B). Orthogonality of ligand response was again observed, with *add*/*xpt* not responding to guanine or PPDA, and M6″/*xpt* showing no response to either guanine or adenine.

dx.doi.org/10.1021/ja502873j | J. Am. Chem. Soc. 2014, 136, 10615−10624

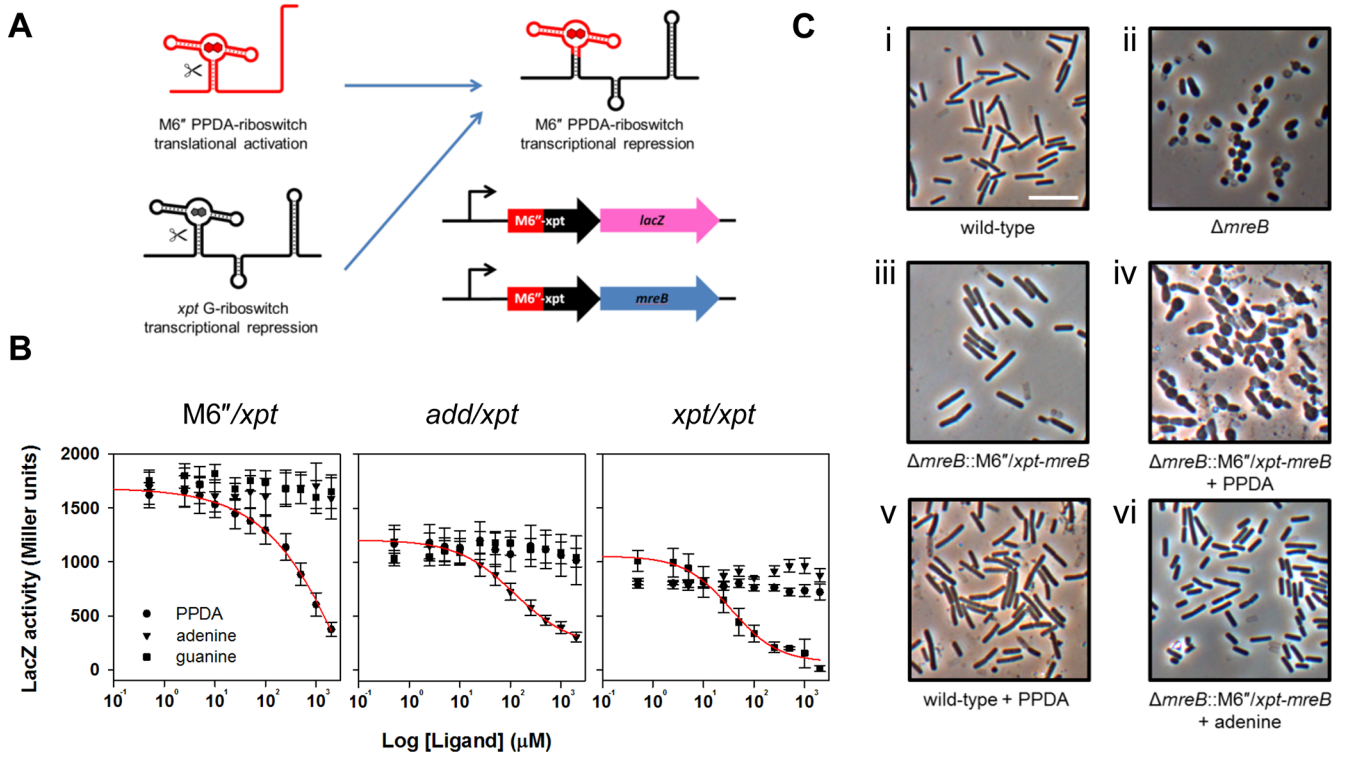

Figure 7. Ligand-dependent repression of gene expression in *B. subtilis*. (A) Chimeric riboswitches were created by fusing the M6″ or *add* A-aptamer (red) to the expression platform of the *xpt* G-riboswitch (black), through a hybrid P1 stem. Expression constructs were created, composed of a constitutive promoter (black line arrow) upstream of a chimeric riboswitch (red/black block arrow), controlling expression of the genes *lacZ* (pink block arrow) or *mreB* (blue block arrow). Constructs were chromosomally integrated. (B) β-galactosidase activity for cells containing repressible *lacZ* constructs, controlled by the indicated chimeric riboswitches, grown in the presence of varying concentrations of PPDA (circles), adenine (triangles), or guanine (squares). Data represent the mean of three repeats, with error bars indicating standard error. Curves were fitted using a four-parameter logistic function. (C) Riboswitch control of *B. subtilis* cell morphology. Wild-type, Δ*mreB*, and Δ*mreB* cells carrying a copy of the *mreB* gene controlled by the repressible M6″/*xpt* chimeric riboswitch were grown in the presence or absence of PPDA or adenine, as indicated. Cells are shown at 60× magnification with the scale bar representing 5 μm.

Significantly, *lacZ* expression levels in the absence of ligand were higher for the M6″/*xpt* strain (ca. 1750 Miller units), than for either the *add*/*xpt* or *xpt*/*xpt* strains (ca. 1250 and ca. 1000 Miller units, respectively). This likely reflects the fact that endogenous levels of adenine and guanine will have a repressive effect on *lacZ* expression in the *add*/*xpt* and *xpt*/*xpt* strains. Consequently, a greater dynamic range of gene expression output was accessible using the repressible M6″−PPDA system, highlighting the advantage of using orthogonal riboswitches which respond to non-natural synthetic ligands. Likewise, the higher EC_{50} for the M6″/*xpt* strain (ca. 500 μM) is probably also a consequence of *lacZ* expression not being already partially repressed before the application of exogenous ligand. These data show that the M6″−PPDA aptamer−ligand system is transferable between Gram-negative (*E. coli*) and Gram-positive (*B. subtilis*) bacteria, and can be utilized as a modular component in the creation of new hybrid riboswitches with diverse gene expression outputs that can be controlled in a dose-dependent manner.

Controlling *B. subtilis* Cell Morphology. To illustrate how the chimeric "transcriptional OFF" switch, M6″/*xpt*, can also regulate the expression of physiologically important native genes, we chose to establish conditional mutants of *mreB* in *B. subtilis*. MreB is an actin homologue which has a critical role in morphogenesis in rod-shaped bacterial species,[32,33] and is an important new target for the development of antimicrobial agents.[34] Wild-type *B. subtilis* adopts a distinctive rod-shaped morphology (Figure 7C-i), whereas cells of the *B. subtilis mreB* deletion strain 3725 (Δ*mreB*) are swollen and round, with compromised growth (Figure 7C-ii).[35] To explore this phenotype further, a copy of the *mreB* gene from the wild-type *B. subtilis* strain 168 was placed under the control of the M6″/*xpt* riboswitch (Figure 7A), and integrated into the chromosome of the Δ*mreB* mutant at the *amyE* locus. The resulting strain (3725C) was able to express *mreB*, complementing the mutant phenotype, to restore the rod-shaped morphology (Figure 7C-iii). The application of PPDA to the 3725C strain repressed *mreB* expression, leading to the reappearance of the swollen round-shaped Δ*mreB* phenotype (Figure 7C-iv). The same concentration of PPDA had no effect on the morphology of the wild-type 168 strain (Figure 7C-v), indicating that the effects of this compound on the 3725C strain were mediated through its interaction with the M6″/*xpt* chimeric riboswitch. Similarly, the rod-shaped morphology of unrepressed 3725C cells was not affected by adenine (Figure 7C-vi), demonstrating once again the *in vivo* ligand-binding orthogonality of the M6″ aptamer. The creation of bacterial strains in which the expression of essential genes can be downregulated, has been widely used in whole-cell screening (WCS) to identify new antibiotics against specific targets and pathways in bacterial pathogens.[36−38] The orthogonal chimeric riboswitches developed here could be deployed to down-regulate antimicrobial targets, such as *mreB*, in a dose-dependent manner at precise time-points in the bacterial

dx.doi.org/10.1021/ja502873j | J. Am. Chem. Soc. 2014, 136, 10615−10624

growth cycle, and thereby find use in sensitive and specific antimicrobial screening regimes or mechanism-of-action studies. Indeed, riboswitch reengineering maybe the best option for WCS in bacterial pathogens where tunable-expression tools are not currently available.

CONCLUSION

Structure-guided chemical genetic screening was successful in identifying superior synthetic ligands for the orthogonal M6″ and M6C″ riboswitches. These ligands, PPDA for M6″ and PPAO for M6C″, exhibit superior *in vivo* reporter gene induction properties, greater *in vitro* affinities, enhanced solubility, and reduced cellular toxicity in comparison to the original ligands.[19] Furthermore, the new riboswitch−ligand pairings are orthogonal, both with one another and with the parental pairing. This was not the case previously, since Amm was capable of inducing both the M6″ and M6C″ riboswitches to a similar extent.[19] Therefore, these new ligand compounds expand the set of mutually orthogonal aptamer−ligand pairs. This could lead to future development of gene regulatory tools based on tandem arrangements of orthogonal riboswitch elements, for example, dual transcriptional and translational control, allowing for more complex regulatory outputs, such as Boolean logic gates.

Both the M6″−PPDA and M6C″−PPAO aptamer−ligand complexes were successfully crystallized and structures were solved at 2.2 Å resolution, revealing a novel proton-linked ligand binding mode that was corroborated through a comprehensive ITC study. This interaction requires the uptake of a single proton between N1 of the ligand and N3 of C51 within the aptamer, thereby alleviating unfavorable electrostatic repulsion. N3 protonation has been described for an active-site cytosine within the HDV ribozyme.[39] Within the context of the folded ribozyme, this cytosine is positioned next to the scissile phosphate group and is H-bonded to another phosphate group through its N4 exocyclic amine group; this environment raises the pK_a of the N3 position from ca. 4.2 to 6.4. In our structures, ligand binding brings the N3 of C51 into close proximity with the N1 lone pair of the ligand, while H-bonding occurs between C47 and the N4 exocyclic amine group of C51; both of these interactions could serve to raise the pK_a at N3 of C51 within the ligand-bound structure. Similarly, methotrexate is protonated at the N1 position of the 2,4-diaminopteridine moiety (a close structural analog of PPDA) when bound as a competitive inhibitor to dihydrofolate reductase,[40] suggesting that PPDA/PPAO could also be protonated at this position. We also found that 2,4-diaminopteridine (PTDA) was capable of activating the M6″ riboswitch, albeit with reduced affinity and lower levels of induction (Figure S9). Pteridines and pyrimido[4,5-*d*]-pyrimidines are pharmacophores that have attracted research interest as antifolate scaffolds, due to their structural similarity to the pterin moiety of folic acid. Variants of our re-engineered riboswitches might therefore be adapted as sensors for antifolate drugs or their metabolic products.

The optimal M6″−PPDA pairing was used to demonstrate how a re-engineered riboswitch can be used to regulate the dose-dependent expression of a physiologically important gene, *cheZ*, required for *E. coli* motility. Furthermore, the modularity, inherent transferability, and precise titratability of orthogonal riboswitches were clearly demonstrated through the creation of a chimeric riboswitch, resulting from the fusion of the M6″ aptamer with the *xpt* G-riboswitch expression platform. In contrast to the "translational ON" M6″ switch employed in the Gram-negative bacterium *E. coli*, the new hybrid M6″/*xpt* riboswitch functions as a "transcriptional OFF" switch to repress the expression of a reporter gene product, β-galactosidase, in a dose-dependent manner in the Gram-positive bacterium *B. subtilis*. Unlike the natural *xpt* G-riboswitch which was repressed by endogenous guanine, the M6″/*xpt* riboswitch exhibits higher levels of expression in the absence of ligand, and therefore a broader dynamic range upon repression with the synthetic non-natural ligand PPDA. The M6″/*xpt* fusion was also used to control expression of the functional gene product MreB, an actin-like protein that is essential for the growth of many rod-shaped bacterial pathogens. Establishing conditional mutants of essential bacterial genes such as *mreB*, using the orthogonal ligand-repressible riboswitches described here, could be valuable in future screening strategies for new antibiotics.

Overall, these studies demonstrate that re-engineered riboswitches can (i) have their *in vivo* performance greatly enhanced through an iterative process of ligand screening and structure determination; (ii) be used to regulate in a precise, dose-dependent manner the expression of native bacterial genes; (iii) be used as modular components of chimeric riboswitch constructs with new regulatory outputs, enabling titratable induction or repression of target gene expression by either translational or transcriptional control; and (iv) form the basis of an array of accessible gene expression tools with inherent transferability between diverse host species, for gene functional analysis and other important biotechnological applications.

MATERIALS AND METHODS

***E. coli* eGFP Reporter Gene Expression Assays.** Plasmids from which the *lac* promoter/operator (P_{lac}) drives the expression of an enhanced green fluorescent protein gene (*eGFP*), under the translational control of a mutant M6″, mutant M6C″, or parental *add* A-riboswitch, were created previously[19] (Figure S10a). For eGFP expression assays, all media contained 50 μg/mL kanamycin. All media were prepared fresh on the day of use and were prewarmed to 37 °C prior to the addition of cells. Cells were grown overnight at 37 °C in LB, diluted 1/20 into M9 medium with or without the addition of IPTG (1 mM), and then incubated for 1 h at 37 °C. M9 cultures were aliquoted (180 μL) onto a 96-well microplate, and riboswitch ligands were added as DMSO solutions (20 μL), with uninduced control samples having an equivalent volume of DMSO added. Data were collected using a multimode detector (Zenyth 3100, Anthos) performing the following cycle at 37 °C: wait 60 s, orbital shake 60 s, read absorbance (620 nm filter), read eGFP fluorescence (using 485 nm excitation and 535 nm emission filters). The cycle was repeated 50 times with data collected throughout (approximately a 4 h run-time). Fluorescence data were divided by the absorbance at 620 nm, to normalize for cell density. Normalized fluorescence values for uninduced cells (no IPTG) were then subtracted from those from induced cells (1 mM IPTG) to account for basal expression in the absence of IPTG. The resulting absolute expression data is presented as normalized fluorescence units (fu/OD). Relative expression levels are presented as induction factors, calculated by dividing the absolute expression levels observed in the presence of ligand by the levels observed in the absence of ligand under the same conditions.

***E. coli* Motility Assays.** To create vectors which express the *E. coli* motility protein CheZ, the *cheZ* gene was PCR amplified from gDNA of *E. coli* RP437 (Coli Genetic Stock Center; CGSC), using the primers cheZ-f and cheZ-r (Table S4). The PCR product was cloned into the P_{lac}-M6″-*eGFP* construct, to create a gene fusion of *cheZ* in-frame with a short 5′-terminal fragment of the eGFP gene, as described previously.[9] This construct was then subcloned into the medium copy number vector pETDuet-1 (Novagen). The resulting pETDuet-(P_{lac}-

dx.doi.org/10.1021/ja502873j | J. Am. Chem. Soc. 2014, 136, 10615−10624

M6″-*cheZ*) vector construct (Figure S10b) was verified by sequencing, then used to transform JW1870 cells (CGSC), a Δ*cheZ* strain of *E. coli*. Overnight LB cultures (containing 50 μg/mL ampicillin) were diluted 1/100 into 2 mL of fresh LB-ampicillin and grown for 8 h at 37 °C. Motility plates (1% tryptone, 0.5% NaCl, 0.25% agar) containing 10 μM IPTG, and varying concentrations of PPDA or adenine (0.1, 0.5, 1, 5, 10, 25, 50, 75, 100, 150, 200, 300, 400, and 500 μM, prepared in DMSO and added to 5% of final volume) were freshly prepared on the day of use. Control plates prepared without ligand, but with an equivalent amount of DMSO, were also prepared with and without 10 μM IPTG. Cell culture (2 μL, approximately 2 × 10^9 cells) was spotted at the center of each motility plate, and then plates were incubated at 25 °C for 24 h. The diameter of cell migration was measured at each ligand concentration, and curves were fitted to this data using a four-parameter logistic function in the SigmaPlot 12 software package (Systat Software). Images of the migration plates were also captured (Figure S7).

Construction of *B. subtilis* Repressible Gene Expression Constructs. DNA fragments encoding a *B. subtilis* σ^A promoter from the *queCDEF* operon,[41] aptamer domains from the *xpt*,[30] *add*[21] and M6″[19] riboswitches, and the expression platform of the *xpt* G-riboswitch, were generated by the 'thermodynamically balanced inside-out' gene synthesis method described by Gao et al.,[42] using a set of five overlapping primer pairs: S1−AS1, S2−AS2, S3−AS3, S4−AS4, and S5−AS5, at concentrations of 200, 120, 80, 60, and 40 nM, respectively, with primers AS4, S5, and AS5 being construct-specific (Table S4). Each of these fragments was cloned separately into the *Eco*RI and *Bam*HI sites of the *B. subtilis* integration vector pDG1661[43] (Bacillus Genomic Stock Center, BGSC), using standard methods, to create a transcriptional fusion with the β-galactosidase reporter gene (*lacZ*). All sequences were verified by DNA sequencing. These vectors (Figure S10c) were used to transform the *B. subtilis* 168 strain (BGSC), with integration into the *amyE* locus using standard methods, to generate the strains termed: *xpt*/*xpt* (*amyE*::pDG1661-P_{queC}-*xpt*/*xpt-lacZ*); *add*/*xpt* (*amyE*::pDG1661-P_{queC}-*add*/*xpt-lacZ*); and M6″/*xpt* (*amyE*::pDG1661-P_{queC}-M6″/*xpt-lacZ*). Integration was confirmed by isolation of the genomic DNA, followed by PCR amplification of the *amyE* locus, then sequencing.

The *mreB* gene was PCR amplified from gDNA of *B. subtilis* 168 (BGSC), using the primers mreB-f and mreB-r, and cloned into the *Eco*RI and *Bam*HI sites of the integration vector pDG1662 (BGSC). Subsequently, a P_{queC}-M6″/*xpt* fragment was amplified from the pDG1661-P_{queC}-M6″/*xpt-lacZ* vector described above, using the primers qmx-f and qmx-r, and cloned into the *Eco*RI and *Bam*HI sites of a separate pDG1662 vector (BGSC). After sequence verification of these constructs, an *amyE*-front fragment containing *mreB* was amplified by primers mreB-f1 and amyEFront-f, and an *amyE*-back fragment containing the P_{queC}-M6″/*xpt* fragment was amplified by primers qmx-r1 and amyEBack-r. An approximately 50 bp linker, composed of sequence derived from the pDG1661 vector, was introduced into both the *amyE*-front and *amyE*-back fragments by the primers Space1 and Space2 respectively. Subsequently, the *amyE*-front and *amyE*-back fragments were fused together by PCR, through their complementary linker sequence, to generate a linear construct with flanking *amyE* front and back sequences for homologous recombination (Figure S10d). All sequences were verified by DNA sequencing. This linear construct was used to transform the *B. subtilis* 3725 strain (Δ*mreB*; kindly provided by Prof. Jeffery Errington), with integration into the *amyE* locus using standard methods, to generate the strain termed 3725C (*amyE*::P_{queC}-M6″/*xpt-mreB*). All cloning primers are listed in (Table S4).

***B. subtilis* β-galactosidase Reporter Gene Assays.** The *B. subtilis* strains *xpt*/*xpt*, *add*/*xpt*, and M6″/*xpt* were grown in LB supplemented with 5 μg/mL chloramphenicol at 37 °C with shaking at 220 rpm overnight. Cultures were diluted 1/20 with fresh LB and used to prepare 200 μL aliquots in a 96 deep-well microplate, containing varying concentrations (0, 0.5, 1, 5, 10, 25, 50, 100, 250, 500, 1000, 2000 μM) of guanine (in 0.1 M KOH), adenine (in H_2O), or PPDA (in H_2O). The equivalent controls without cells were also prepared. One M MES, pH 6, was added to samples containing guanine to restore the pH of the media to pH 7. Samples were incubated for 4 h at 37 °C with shaking at 500 rpm, harvested by centrifugation at 1750*g* for 20 min at 4 °C, and then resuspended in 200 μL of phosphate-buffered saline (PBS). A total of 100 μL of each sample was transferred to a clear-bottomed 96-well microplate, and the OD_{600} was measured using a SynergyHT platereader (BioTek). OD_{600} values were corrected using the control samples without cells. Cells were lysed by the addition of 100 μL of PBS containing 2 μg of lysozyme and 2× PopCulture (Merck), then incubated at room temperature for 15 min. Miller assays were carried out essentially as originally described by Miller.[44] Briefly, 10 μL of lysate was added to 132.5 μL of Z buffer (60 mM Na_2HPO_4, 40 mM NaH_2PO_4, 10 mM KCl, 1 mM $MgSO_4$, 50 mM β-mercaptoethanol, pH 7.0) in a clear-bottomed 96-well microplate. The reaction was started by the addition of 29 μL of 4 mg/mL *o*-nitrophenyl-β-D-galactoside (ONPG) and allowed to proceed at room temperature for 45 min. The reaction was stopped by adding 75 μL of 1 M Na_2CO_3. The absorbance at 420 and 550 nm wavelengths was measured using the SynergyHT platereader, and the values were corrected using the control samples without cells. Miller units were calculated by the following equation:

$$\frac{1000 \times (A_{420} - 1.75 \times A_{550})}{OD_{600} \times t \times v}$$

where t is the length of incubation in minutes and v is the volume of lysate (in mL). To determine the EC_{50}, curves were fit to the data using a four-parameter logistic function, in the SigmaPlot 12 software package (Systat Software).

***B. subtilis* Cell Morphology Assays.** *B. subtilis* wild-type (168 strain), Δ*mreB* (3725 strain), and Δ*mreB* cells complemented with an M6″/*xpt*-controlled *mreB* construct (3725C strain) were grown for 5 h in nutrient broth (with 25 mM $MgCl_2$) in the presence or absence of 2 mM PPDA or adenine. Cells were pelleted by centrifugation at 2400*g* for 5 min, washed twice with nutrient broth to remove magnesium, and incubated for 30 min at 37 °C with shaking at 200 rpm. Cultures were then left at 37 °C for 6 h to allow any mutant morphological phenotype to develop. Cells were harvested by centrifugation at 2400*g* for 5 min and resuspended in a small volume of supernatant before being transferred to poly-L-lysine coated slides. Cells were visualized at 60× magnification by phase contrast microscopy (Olympus BX51).

***in vitro* Transcription of RNA Aptamer Domains.** To produce *in vitro* transcribed riboswitch aptamers, we created linear dsDNA templates containing the minimal T7 promoter and 71 nt riboswitch template, as described previously.[19] Oligonucleotide primers were purchased from Sigma, and PCR reactions were performed using Phusion high-fidelity DNA polymerase (NEB), following the manufacturers recommended procedures. The *in vitro* transcription reaction was performed with T7 RNA polymerase (prepared in-house), following established methods.[45] Upon completion (4−6 h at 37 °C), the reaction was treated with DNase I (NEB, 10 U/mL for 30 min at 37 °C), then EDTA (0.5 M, pH 8.0) was added until solutions were cleared of precipitate. To avoid denaturing the RNA, transcribed aptamers were separated from failed transcription products and NTPs under native conditions by size-exclusion chromatography. Samples were loaded onto an ÄKTA Explorer system equipped with a HiLoad 26/600 Superdex 200 PG column (GE Healthcare), and eluted isocratically in 50 mM HEPES pH 7.5, 100 mM KCl, 20 mM $MgCl_2$ at a flow rate of 2.0 mL/min. Fractions were collected and assessed for purity by denaturing PAGE (8.0 M urea, 12% polyacrylamide gel), then combined and prepared as described for ITC and crystallization trials.

Isothermal Titration Calorimetry. Riboswitch aptamer domains, purified from *in vitro* transcription reactions, were dialyzed overnight at 4 °C into 50 mM buffer (HEPES, PIPES or TRIS, as described in figure legends) pH 7.5, 20 mM $MgCl_2$, 100 mM KCl. Dry ligand compounds were then dissolved in the same dialysis buffer. Samples were degassed and ITC experiments were performed on a VP-ITC microcalorimeter (MicroCal) at 25 °C with a reference power of 5 μcal/s, using a cell concentration of 8.8 μM RNA aptamer and a titrant concentration of 100 μM ligand. An initial 2 μL (4.8 s) injection was

followed by 24 12 μL (28.8 s) injections, with a 6 min delay between injections. Control runs were performed in which ligand was injected into dialysis buffer, and data from these runs was subtracted from the experimental data prior to curve fitting in Origin, using the supplied software (MicroCal).

X-ray Crystallography and Structure Determination. Riboswitch aptamer domains, purified from *in vitro* transcription reactions, were dialyzed overnight at 4 °C into 50 mM HEPES pH 7.5, 5 mM $MgCl_2$, 100 mM KCl. Dry ligand compounds were then dissolved in the same dialysis buffer. Aptamer and ligand solutions were combined in a 1:10 ratio of concentration and incubated on ice for 30 min prior to centrifugal concentration to a final concentration of ca. 0.4 mM RNA−ligand complex. Co-crystallization of these complexes was performed as previously described.[21] Rod shaped crystals reached their maximum dimensions (~30 × 30 × 500 μm) in approximately 7−10 days at 20 °C. Crystals were cryoprotected by transferring to the same solution supplemented with 15% Glycerol and flash cooled by immersion in liquid nitrogen. Diffraction data were collected at the Diamond Light Source, UK national synchrotron facility (Oxfordshire), and processed with the XDS package.[46] Structures were solved by molecular replacement with the CCP4 program Phaser,[47] using the M6C″ aptamer structure (3LA5.pdb) as a starting model. To reduce model bias, the new structures were subjected to initial rounds of simulated annealing followed by rigid body and restrained refinement with Phenix.refine.[48] Ordered solvent molecules were added using Phenix.refine and manual model building was carried out with Coot.[49] Data and final model statistics are given in (Table S2a). Coordinates and structure factors have been deposited into the RSCB protein databank (PDB accession codes 4LX5 for M6″−PPDA and 4LX6 for M6C″−PPAO).

■ ASSOCIATED CONTENT

Supporting Information

Analytical data for synthetic ligands, 10 additional figures (Figures S1−S10) and four tables of data (Tables S1−S4). This material is available free of charge via the Internet at http://pubs.acs.org.

■ AUTHOR INFORMATION

Corresponding Author

jason.micklefield@manchester.ac.uk.

Author Contributions

‖These authors contributed equally.

Notes

The authors declare no competing financial interest.

■ ACKNOWLEDGMENTS

This work was supported by the BBSRC (Grant BB/I012648/1). The EPSRC provided a PhD studentship award (for P.T.L.). We thank Prof. Jeffery Errington for providing the *B. subtilis* 3725 strain, Dr. Neil Dixon for helpful discussions and Dr. Majid Al Nakeeb for technical support.

■ REFERENCES

(1) Breaker, R. *Cold Spring Harbor Perspect. Biol.* **2012**, *4*, No. a003566.
(2) Serganov, A.; Nudler, E. *Cell* **2013**, *152*, 17.
(3) Garst, A. D.; Edwards, A. L.; Batey, R. T. *Cold Spring Harbor Perspect. Biol.* **2011**, *3*, No. a03533.
(4) Ceres, P.; Garst, A. D.; Marcano-Velazquez, J. G.; Batey, R. T. *ACS Synth. Biol.* **2013**, *2*, 463.
(5) Ceres, P.; Trausch, J. J.; Batey, R. T. *Nucleic Acids Res.* **2013**, *41*, 10449.
(6) Sudarsan, N.; Hammond, M. C.; Block, K. F.; Welz, R.; Barrick, J. E.; Roth, A.; Breaker, R. R. *Science* **2006**, *314*, 300.
(7) Khlebnikov, A.; Keasling, J. D. *Biotechnol. Prog.* **2002**, *18*, 672.
(8) Morgan-Kiss, R. M.; Wadler, C.; Cronan, J. E., Jr. *Proc. Natl. Acad. Sci. U.S.A.* **2002**, *99*, 7373.
(9) Dixon, N.; Robinson, C. J.; Geerlings, T.; Duncan, J. N.; Drummond, S. P.; Micklefield, J. *Angew. Chem., Int. Ed.* **2012**, *51*, 3620.
(10) Vinkenborg, J. L.; Karnowski, N.; Famulok, M. *Nat. Chem. Biol.* **2011**, *7*, 519.
(11) Wittmann, A.; Suess, B. *FEBS Lett.* **2012**, *586*, 2076.
(12) Fowler, C. C.; Brown, E. D.; Li, Y. *ChemBioChem* **2008**, *9*, 1906.
(13) Lynch, S. A.; Gallivan, J. P. *Nucleic Acids Res.* **2009**, *37*, 184.
(14) Saragliadis, A.; Klauser, B.; Hartig, J. S. *Methods Mol. Biol.* **2012**, *848*, 455.
(15) Sharma, V.; Nomura, Y.; Yokobayashi, Y. *J. Am. Chem. Soc.* **2008**, *130*, 16310.
(16) Topp, S.; Gallivan, J. P. *ChemBioChem* **2008**, *9*, 210.
(17) Nomura, Y.; Zhou, L.; Miu, A.; Yokobayashi, Y. *ACS Synth. Biol.* **2013**, *2*, 684.
(18) Wieland, M.; Benz, A.; Klauser, B.; Hartig, J. S. *Angew. Chem., Int. Ed.* **2009**, *48*, 2715.
(19) Dixon, N.; Duncan, J. N.; Geerlings, T.; Dunstan, M. S.; McCarthy, J. E.; Leys, D.; Micklefield, J. *Proc. Natl. Acad. Sci. U.S.A.* **2010**, *107*, 2830.
(20) Reining, A.; Nozinovic, S.; Schlepckow, K.; Buhr, F.; Furtig, B.; Schwalbe, H. *Nature* **2013**, *499*, 355.
(21) Serganov, A.; Yuan, Y. R.; Pikovskaya, O.; Polonskaia, A.; Malinina, L.; Phan, A. T.; Hobartner, C.; Micura, R.; Breaker, R. R.; Patel, D. J. *Chem. Biol.* **2004**, *11*, 1729.
(22) Gilbert, S. D.; Reyes, F. E.; Edwards, A. L.; Batey, R. T. *Structure* **2009**, *17*, 857.
(23) Beres, L.; Sturtevant, J. M. *Biochemistry* **1971**, *10*, 2120.
(24) Fukada, H.; Takahashi, K. *Proteins* **1998**, *33*, 159.
(25) Baker, B. M.; Murphy, K. P. *Biophys. J.* **1996**, *71*, 2049.
(26) Gomez, J.; Freire, E. *J. Mol. Biol.* **1995**, *252*, 337.
(27) Raman, C. S.; Allen, M. J.; Nall, B. T. *Biochemistry* **1995**, *34*, 5831.
(28) Porter, S. L.; Wadhams, G. H.; Armitage, J. P. *Nat. Rev. Microbiol.* **2011**, *9*, 153.
(29) Topp, S.; Gallivan, J. P. *J. Am. Chem. Soc.* **2007**, *129*, 6807.
(30) Batey, R. T.; Gilbert, S. D.; Montange, R. K. *Nature* **2004**, *432*, 411.
(31) Mandal, M.; Boese, B.; Barrick, J. E.; Winkler, W. C.; Breaker, R. R. *Cell* **2003**, *113*, 577.
(32) Dominguez-Escobar, J.; Chastanet, A.; Crevenna, A. H.; Fromion, V.; Wedlich-Soldner, R.; Carballido-Lopez, R. *Science* **2011**, *333*, 225.
(33) Garner, E. C.; Bernard, R.; Wang, W.; Zhuang, X.; Rudner, D. Z.; Mitchison, T. *Science* **2011**, *333*, 222.
(34) Bean, G. J.; Flickinger, S. T.; Westler, W. M.; McCully, M. E.; Sept, D.; Weibel, D. B.; Amann, K. J. *Biochemistry* **2009**, *48*, 4852.
(35) Formstone, A.; Errington, J. *Mol. Microbiol.* **2005**, *55*, 1646.
(36) Abrahams, G. L.; Kumar, A.; Savvi, S.; Hung, A. W.; Wen, S.; Abell, C.; Barry, C. E., III; Sherman, D. R.; Boshoff, H. I.; Mizrahi, V. *Chem. Biol.* **2012**, *19*, 844.
(37) Singh, S. B.; Phillips, J. W.; Wang, J. *Curr. Opin. Drug Discovery Dev.* **2007**, *10*, 160.
(38) Wang, J.; Soisson, S. M.; Young, K.; Shoop, W.; Kodali, S.; Galgoci, A.; Painter, R.; Parthasarathy, G.; Tang, Y. S.; Cummings, R.; Ha, S.; Dorso, K.; Motyl, M.; Jayasuriya, H.; Ondeyka, J.; Herath, K.; Zhang, C.; Hernandez, L.; Allocco, J.; Basilio, A.; Tormo, J. R.; Genilloud, O.; Vicente, F.; Pelaez, F.; Colwell, L.; Lee, S. H.; Michael, B.; Felcetto, T.; Gill, C.; Silver, L. L.; Hermes, J. D.; Bartizal, K.; Barrett, J.; Schmatz, D.; Becker, J. W.; Cully, D.; Singh, S. B. *Nature* **2006**, *441*, 358.
(39) Gong, B.; Chen, J. H.; Chase, E.; Chadalavada, D. M.; Yajima, R.; Golden, B. L.; Bevilacqua, P. C.; Carey, P. R. *J. Am. Chem. Soc.* **2007**, *129*, 13335.
(40) Cocco, L.; Roth, B.; Temple, C., Jr.; Montgomery, J. A.; London, R. E.; Blakley, R. L. *Arch. Biochem. Biophys.* **1983**, *226*, 567.
(41) Reader, J. S.; Metzgar, D.; Schimmel, P.; de Crecy-Lagard, V. *J. Biol. Chem.* **2004**, *279*, 6280.

(42) Gao, X.; Yo, P.; Keith, A.; Ragan, T. J.; Harris, T. K. *Nucleic Acids Res.* **2003**, *31*, e143.
(43) Guerout-Fleury, A. M.; Frandsen, N.; Stragier, P. *Gene* **1996**, *180*, 57.
(44) Miller, J. H. In *Experiments in Molecular Genetics*; Miller, J. H., Ed.; Cold Spring Harbor Laboratory Press: Cold Spring Harbor, NY, 1972; p 352.
(45) Gilbert, S. D.; Mediatore, S. J.; Batey, R. T. *J. Am. Chem. Soc.* **2006**, *128*, 14214.
(46) Kabsch, W. *J. Appl. Crystallogr.* **1993**, *26*, 795.
(47) McCoy, A. J.; Grosse-Kunstleve, R. W.; Adams, P. D.; Winn, M. D.; Storoni, L. C.; Read, R. J. *J. Appl. Crystallogr.* **2007**, *40*, 658.
(48) Adams, P. D.; Grosse-Kunstleve, R. W.; Hung, L. W.; Ioerger, T. R.; McCoy, A. J.; Moriarty, N. W.; Read, R. J.; Sacchettini, J. C.; Sauter, N. K.; Terwilliger, T. C. *Acta Crystallogr., Sect. D* **2002**, *58*, 1948.
(49) Emsley, P.; Cowtan, K. *Acta Crystallogr., Sect D* **2004**, *60*, 2126.